Cation- and anion-ordered rutile-type derivative $LiTeO_3(OH)$
Electronic Supplementary information (ESI)

Kotaro Fujii,[a] Yume Yoshida,[b] Yue Jin Shan,[b] Keitaro Tezuka,[b] Yoshiyuki Inaguma,[c] Masatomo Yashima[a,*]

a Department of Chemistry, School of Science, Tokyo Institute of Technology, 2-12-1-W4-17, O-okayama, Meguro-ku, Tokyo, 152-8551, Japan
b Department of Applied Chemistry, Faculty of Engineering, Utsunomiya University, 7-1-2 Yoto, Utsunomiya, Tochigi 321-8585, Japan
c Department of Chemistry, Faculty of Science, Gakushuin University, 1-5-1 Mejiro, Toshima-ku, Tokyo 171-8588, Japan

* Corresponding author (M. Y.): yashima@cms.titech.ac.jp

(A) Structure map for MX_2 compounds

In 1981, Burdett et al. reported the structure map for MX_2 compounds based on the atomic radii of M and X atoms.[24] Here, we revised this map using the ionic radii (Fig. S1). r_M and r_X are the ionic radii of cation M and anion X, respectively. $LiTeO_3(OH)$ exists in the region of rutile-type structure (Red cross mark in Fig. S1).

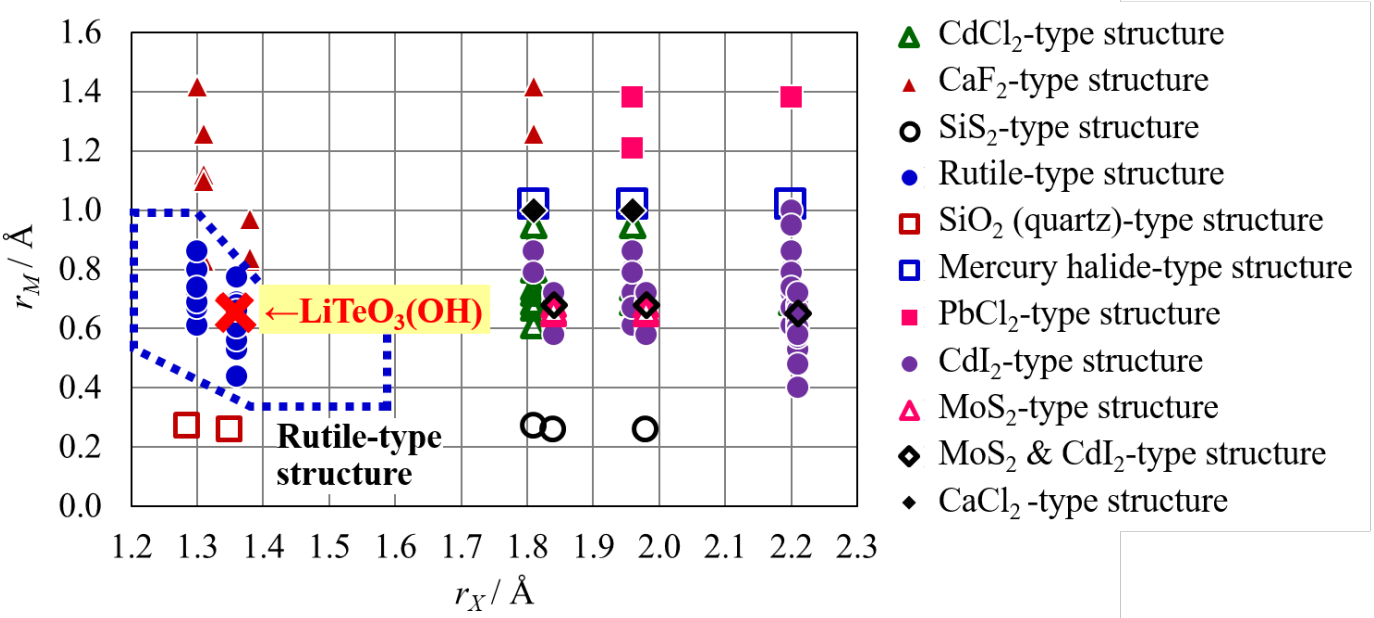

Fig. S1. Structure map for MX_2 compounds. r_M and r_X are ionic radii of cation M and anion X, respectively. Ionic radii after Shannon (R. D. Shannon, Acta Crystallogr. A, 32, 751-767, 1976)) were used.

(B) Estimation of OH^- content

OH^- content in $LiTeO_3(OH)$ was estimated by the following method. 6.6% weight loss was observed for $LiTeO_3(OH)$ during the heating up to 600 °C by thermogravimetric (TG) analysis. After heating at 600 °C, $LiTeO_3(OH)$ was decomposed into Li_2TeO_4 and TeO_2, which were confirmed from X-ray powder diffraction measurements. Therefore, the following reaction occurred by heating at 600 °C,

$$2\ LiTeO_3(OH) \rightarrow Li_2TeO_4 + TeO_2 + 1/2\ O_2 + H_2O,$$

because the weight loss in this reaction 6.51% agreed well with the observed weight loss 6.6%.

(C) SHG measurement

The optical second harmonic generation (SHG) response was measured for $LiTeO_3(OH)$ powders at ambient temperature using a Continuum Minilite II YAG : Nd laser (λ = 1064 nm). The details of the apparatus are described in our previous work*. As shown in Fig. S2, SHG signal was observed.

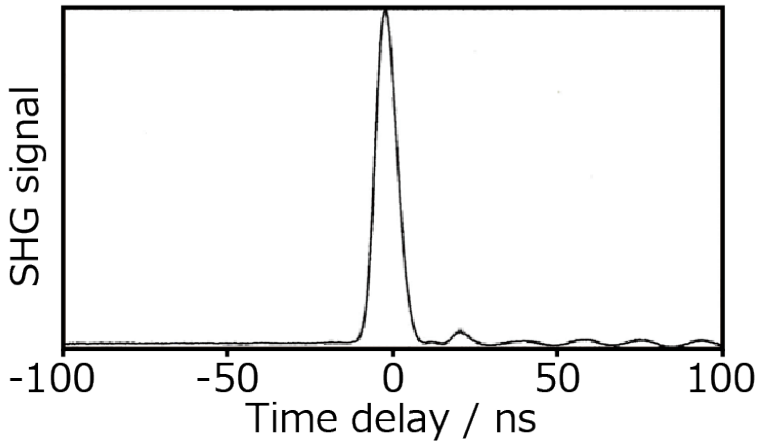

Fig. S2. Plot of SHG signal for $LiTeO_3(OH)$ measured at ambient temperature.

* Y. Inaguma, A. Aimi, Y. Shirako, D. Sakurai, D. Mori, H. Kojitani, M. Akaogi and M. Nakayama, *J. Am. Chem. Soc.*, 2014, **136**, 2748-2756.

(D) Refined structural parameters of $LiTeO_3(OH)$

Table S1. Crystallographic data of $LiTeO_3(OH)$

	ND		SCXRD
Chemical formula		$LiTeO_3(OH)$	
Temperature / °C	27		24
d range / Å	0.7 − 6.0	Wavelength / Å	0.71073
Space group		$P2_1$	
a / Å	5.320533(3)		5.3284(4)
b / Å	4.891622(2)		4.8924(3)
c / Å	5.341556(2)		5.3418(5)
α / °	90		90
β / °	109.497811(5)		109.455(9)
γ / °	90		90
V / Å^3	131.0473(4)		131.303(19)
Calculated density / g cm^{-3}	5.057		5.047
		Crystal size / μm	13 × 10 × 5
R_{wp}	0.0139	R_{int}	0.0427
R_p	0.0119	R_{sigma}	0.0479
R_B	0.0325	wR_2	0.0663
R_F	0.0398	R_1 ($I > 2\sigma(I)$)	0.0299
Goodness of fit	2.363		1.117

The Flack parameter[33] was refined to be 0.44(17) for the SCXRD data using the twin matrix $\begin{pmatrix} -1 & 0 & 0 \\ 0 & -1 & 0 \\ 0 & 0 & -1 \end{pmatrix}$, which indicated both structures related by the inversion center exist equally in the crystal of $LiTeO_3(OH)$ (i.e. racemic twin).

Table S2. Refined structural parameters of $LiTeO_3(OH)$ using the ND data taken at 27 °C. All atoms are located at the Wyckoff general site 2*a*. Isotropic atomic displacement parameters (ADPs) were constrained to be U_{iso}(O1) = U_{iso}(O2), and U_{iso}(O3) = U_{iso}(O4), because these are related by the pseudo-inversion center.

Site label	Atom	g*	x	y	z	U_{iso}**	BVS***
Li	Li	1	0.73073(2)	0.97042(3)	0.48934(18)	0.02591320(10)	1.04
Te	Te	1	0.74531(6)	0.47459(10)	−0.01025(5)	0.0022003(2)	6.00
O1	O	1	0.59455(7)	0.1643(8)	0.11791(5)	0.005379(19)	2.05
O2	O	1	0.91107(6)	0.78974(8)	−0.11018(5)	= U_{iso}(O1)	2.00
O3	O	1	0.64606(6)	0.34405(7)	−0.34382(5)	0.0077343(2)	2.11
O4	O	1	0.85143(7)	0.60982(7)	0.35631(5)	= U_{iso}(O3)	1.85
H	H	1	0.76335(6)	0.5****	0.45625(5)	0.01952314(5)	0.98

* g: occupancy factor

** U_{iso}: Isotropic atomic displacement parameter

*** BVS : Bond valence sum

**** y of H atom was fixed to 0.5 because the space group is $P2_1$.

Table S3. Refined structural parameters of $LiTeO_3(OH)$ using the SCXRD data taken at 24 °C.

Site label	Atom	*g*	*x*	*y*	*z*	U_{iso}	BVS
Li	Li	1	0.756(5)	0.96(3)	0.500(3)	0.019(4)	1.04
Te	Te	1	0.75204(14)	0.456(4)	0.00683(11)	0.00557(16)	5.90
O1	O	1	0.5925(16)	0.1435(18)	0.1155(12)	0.0068(8)	2.02
O2	O	1	0.9081(16)	0.7709(18)	−0.1174(12)	0.0068(8)	1.99
O3	O	1	0.6477(17)	0.3258(16)	−0.3471(12)	0.0075(8)	1.72
O4	O	1	0.8549(15)	0.5922(16)	0.3526(12)	0.0075(8)	2.19
H	H	1	0.76335	0.5	0.45625	0.019	0.98

(E) Details and results of the DFT calculations

The generalized gradient approximation (GGA) electronic calculation was carried out with Vienna Ab initio Simulation Package (VASP), in order to study the optimized structure of $LiTeO_3(OH)$ using projector augmented-wave (PAW) potentials for Li, H, Te, and O atoms. A plane-wave basis set with a cutoff of 500 eV was used. The Perdew-Burke-Ernzerhof (PBE) GGA was employed for the exchange and correlation functionals. Sums over occupied electronic states were performed using the Monkhorst-Pack scheme on a 7 × 7 × 7 set of a *k*-point mesh. Unit-cell parameters and atomic coordinates were optimized with the convergence condition of 0.02 eV $Å^{-1}$. The positions of all atoms were relaxed in the space group $P2_1$. The calculated Born effective charge tensor is shown in Table S5. The calculated band structure of $LiTeO_3(OH)$ showed the direct band gap (Fig. S3).

Table S4. Optimized structural parameters of $LiTeO_3(OH)$ by the DFT calculation. Optimized lattice parameters: a = 5.4008 Å, b = 4.9830 Å, c = 5.4074 Å, α = 90 °, β= 109.38 °, γ = 90 °, V = 137.29 $Å^3$.

Site label	Atom	*x*	*y*	*z*
Li	Li	0.73734	0.98771	0.51201
Te	Te	0.74608	0.46829	0.98719
O1	O	0.59412	0.16207	0.12276
O2	O	0.90629	0.78957	0.88401
O3	O	0.64336	0.34264	0.64222
O4	O	0.85374	0.60657	0.34637
H	H	0.7656	0.49626	0.45669

Table S5. Calculated Born effective charge tensor for $LiTeO_3(OH)$

*Z**	*xx*	*yy*	*zz*	*xy*	*xz*	*yx*	*yz*	*zx*	*zy*
Te	6.179	5.704	4.037	0.838	−0.222	−0.850	−1.375	0.031	0.244
Li	1.028	1.225	1.376	−0.082	0.113	−0.249	−0.096	0.144	0.215
O1	−2.392	−2.207	−1.369	−1.023	0.031	−0.999	0.119	0.030	0.157
O2	−2.426	−2.241	−1.268	−1.014	−0.163	−0.983	0.047	−0.142	0.064
O3	−1.675	−1.563	−2.109	−0.061	0.353	0.140	0.075	0.385	0.037
O4	−1.612	−1.359	−2.030	−0.213	0.380	0.087	−0.043	0.590	0.250
H	0.898	0.441	1.363	0.522	−0.492	0.102	−0.102	−1.038	−0.843

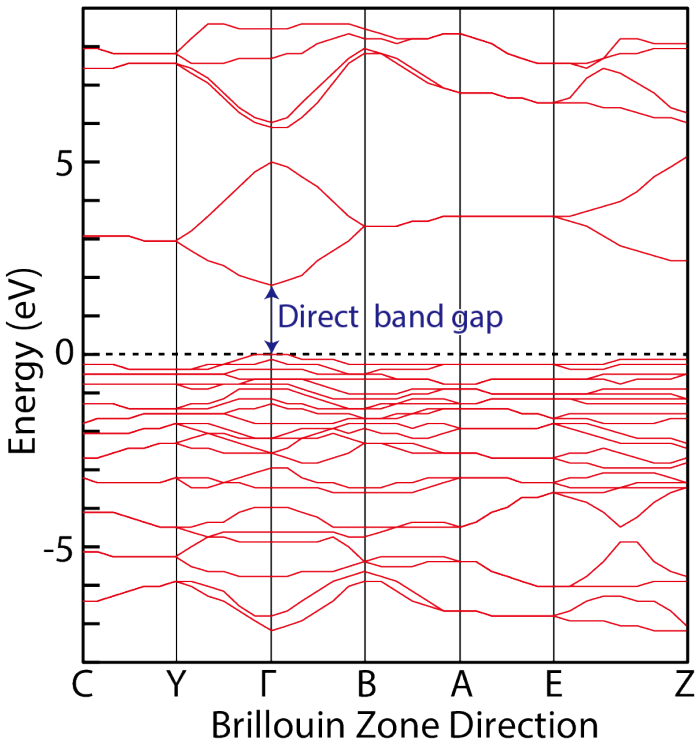

Fig. S3. Calculated band structure of $LiTeO_3(OH)$.

(F) Comparison of the distortion parameters

The polarization value of $LiTeO_3(OH)$ is calculated to be 1.36(15) μC cm^{-2} along the *b* axis. Contributions of Li^+, Te^{6+}, and H^+ cations to the polarization value are 0.96, −1.21, and 1.62 μC cm^{-2}, respectively (average position of four oxygen atoms were set to the origin in this calculation). It is known that displacements of cation *M* (*M* = Ti or Nb) from the center of MO_6 octahedra are important for large polarizations for some materials such as $LiNbO_3$-type $ZnTiO_3$ and $LiNbO_3$.[27] In the present case, however, the distortion of $LiO_4(OH)_2$ and TeO_5OH

octahedra are smaller than those of TiO_6 and NbO_6 in $LiNbO_3$-type $ZnTiO_3$ and $LiNbO_3$, respectively. Degrees of distortions of MO_6 octahedra were calculated using following octahedral distortion parameter Δ.**

$$\Delta = \frac{1}{6}\sum_{i=1}^{6}\left\{\frac{(d_i - d_{\mathrm{ave}})}{d_{\mathrm{ave}}}\right\}^2$$

Here, d_i is the atomic distance of M−O, and d_{ave} is the average of six d_i. Δ of $LiO_4(OH)_2$ and TeO_5OH octahedra are calculated to be 13×10^{-4}, and 8×10^{-4}, respectively. These are smaller than those of TiO_6 octahedra ($\Delta = 47\times10^{-4}$) in $LiNbO_3$-type $ZnTiO_3$, and NbO_6 octahedra ($\Delta = 40\times10^{-4}$) in $LiNbO_3$-type $LiNbO_3$, which are known to have polar structures by the second-order Jahn-Teller effect.[27]

* Y. Inaguma, A. Aimi, Y. Shirako, D. Sakurai, D. Mori, H. Kojitani, M. Akaogi and M. Nakayama, *J. Am. Chem. Soc.*, 2014, **136**, 2748-2756.
** I. D. Brown, R. D. Shannon, *Acta Crystallogr., Sect. A* 1973, **29**, 266-282.

(G) Results of the BVE calculations for Li^+, H^+, and O^{2-}

In order to investigate the possibility of $LiTeO_3(OH)$ as an ionic conductor, the BVE calculations were performed using the refined crystal structure from the neutron diffraction data of $LiTeO_3(OH)$. Table S6 summarized the BVE barriers for the Li^+, H^+, and O^{2-} migrations along the *a*, *b* and *c* axes. The BVE barrier for Li^+ migration is significantly larger than the others. Therefore, $LiTeO_3(OH)$ is not good candidate for the Li^+ conductor. The high BVE barrier for Li^+ migration is ascribed to the small bottleneck size of the Li^+ migration path. As shown in Fig. S4, the bottleneck of Li^+ migration along the *b* aixs is at the center of the O1-O3-O3 triangle (sky-blue triangle). The critical radius of the O1-O3-O3 triangle is 0.26 Å, which is significantly smaller than the ionic radius of Li^+ (0.76 Å for CN = 6). Therefore, Li^+ is difficult to migrate in the crystal structure of $LiTeO_3(OH)$. The BVE barrier for the H^+

migration along the *b* axis (0.38 eV) is lower than those of along the *a* and *c* axes, suggesting one dimensional proton conduction would occur in $LiTeO_3(OH)$. The BVE barriers for the O^{2-} migration along the *a*, *b*, and *c* axes are comparable and range from 0.79 to 1.01 eV. Thus, $LiTeO_3(OH)$ is also a good candidate for oxide-ion conductor, with three dimensional oxide-ion migration path.

Table S6. BVE barriers for the Li^+, H^+, and O^{2-} migrations along the *a*, *b* and *c* axes

	a axis (eV)	*b* axis (eV)	*c* axis (eV)
Li^+	3.05	2.80	5.60
H^+	0.69	0.38	0.64
O^{2-}	1.01	0.79	0.84

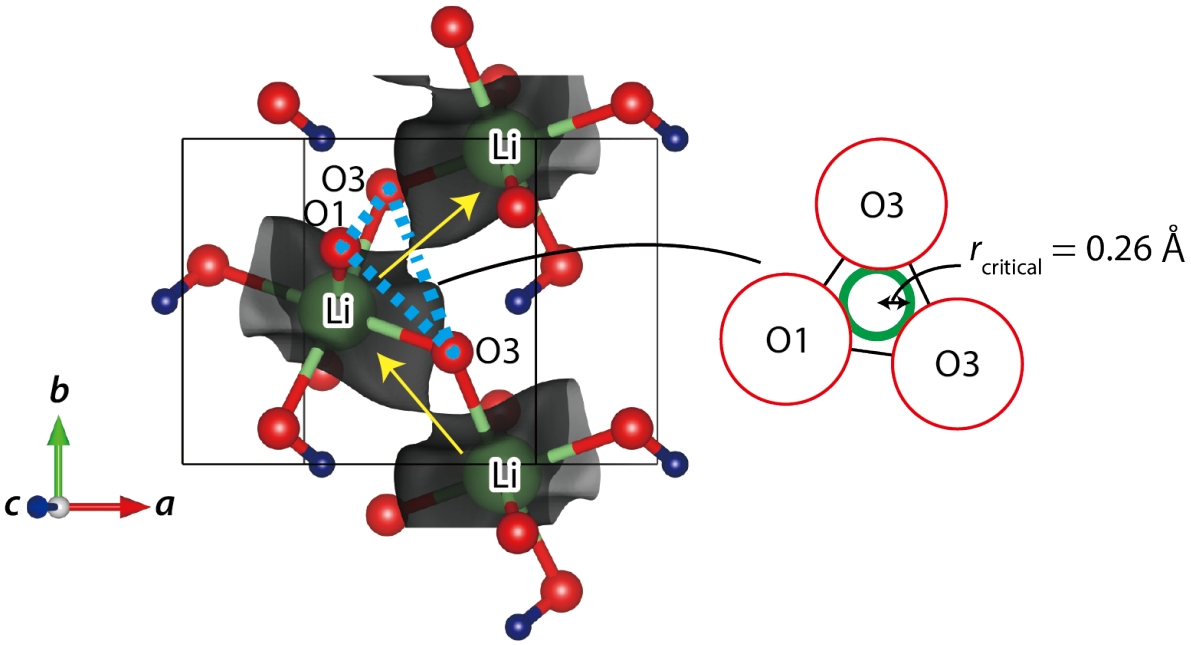

Fig. S4. Bond-valence-based energy (BVE) landscape for a Li^+ in $LiTeO_3(OH)$ with black isosurfaces at 2.8 eV. Yellow arrows indicate the possible Li^+ migration path along the *b*-axis. Light-blue triangle represents the bottleneck for the Li^+ migration.